Prediction of Global VLE for Mixtures with Improved Renormalization Group Theory

Jianguo Mi, Chongli Zhong, and Yi-Gui Li
Dept. of Chemical Engineering, The Key Laboratory of Bioprocess of Beijing, Beijing University of Chemical Technology, Beijing 100029, China

Yiping Tang
Honeywell Process Solutions, London, Ontario N6A 6K2, Canada

DOI 10.1002/aic.10581
Published online September 7, 2005 in Wiley InterScience (www.interscience.wiley.com).

The recently proposed renormalization group (RG) theory is reformulated within the context of density functional theory and applied to predicting global vapor–liquid equilibria (VLE) of Lennard–Jones chain pure fluids and fluid mixtures. An accurate equation based on the solution of the first-order mean-sphere approximation (FMSA) is adopted outside the critical region. Inside the critical region, the direct correlation function of FMSA is incorporated into the new RG transformation to describe the long-range fluctuation, which is conformal to general inhomogeneous studies. The new RG theory is applied to correcting real mixture phase envelopes, as well as corresponding phase diagrams of pure compounds for the critical region. The calculated results are in substantial agreement with those from experiment and molecular simulation both inside and outside the critical region. The new method is highly predictive because no adjustable parameters and no mixing rule are needed for both model and real fluid mixtures. © 2005 American Institute of Chemical Engineers *AIChE J,* 52: 342–353, 2006
Keywords: prediction, VLE, mixture, renormalization group theory, density functional theory

Introduction

An accurate prediction of thermodynamic properties of fluid mixtures both inside and outside the critical region represents one of the important goals in chemical and related industries. The subject has been investigated intensively for decades. Although considerable progress was made in description or correction of vapor–liquid equilibria (VLE), it has been difficult to develop a universal model to predict behavior for mixture phase based solely on knowledge of the molecular structure and intermolecular forces from the pure component.

Molecular simulation provides a promising route. In recent years, many computer simulations of phase equilibria of mixtures have appeared in the literature. These simulations are mostly focused on the VLE of the Lennard–Jones (LJ) fluid. The VLE had been simulated with the Monte Carlo method,[1] molecular dynamic method,[2] and at some extreme potential parameter ratios.[3] Simulations have proved useful for testing theories as well as for developing general intuition regarding the influence of molecular size and intermolecular interaction on phase behavior.[4,5]

An alternative approach is equation of state (EOS), which aimed to provide a general description of phase behavior for broad classes of substances. A multitude of EOSs have been developed based on classical homogeneous fluid theories. Many engineering cubic EOSs are based on the van der Waals equation, such as Redlich–Kwong (RK),[6] Soave–Redlich–Kwong (SRK),[7] and Peng–Robinson (PR).[8] However, the EOS has some limitations: inaccurate liquid densities and thermodynamic properties and phase behavior at high pressures, in-

Correspondence concerning this article should be addressed to C.-L. Zhong at zhongcl@mail.buct.edu.cn *or* zhongcl88@yahoo.com.

© 2005 American Institute of Chemical Engineers

cluding the critical region, that are difficult to describe. A review about these equations was given by Wei and Sadus.[9] A semiempirical approach for EOSs is to use the fully fitting equations. They are derived with an optimization process that fits the most useful terms from experimental data[10] or molecular simulation data.[11,12] The fitting equations are useful in practical applications. The crucial disadvantage of such fitting equations is their restriction to pure fluids and poor predictive ability. At present, EOSs developed from statistical mechanics find their applications in chemical engineering for characterizing the thermodynamic behavior of mixtures including VLE. The statistical associating fluid theory (SAFT)[13,14] has been investigated extensively since it was first proposed. SAFT EOSs are advantageous over cubic and semiempirical EOSs by covering many more types of fluids and by providing more consistent thermodynamics. The EOSs developed by Chapman et al.[15] and by Huang and Radosz[16,17] are two earlier examples.

Since then, many modifications of the SAFT EOS were suggested over the years, such as LJ–SAFT[18-21] and perturbed-chain (PC)–SAFT.[22,23] Although these practical calculations yield encouraging results, their further improvement is narrow: underlying fittings are subject to the availability of simulation data and their good quality is often limited to a certain region. In addition, a common dissatisfaction in these models is their accompanying mixing rules. These mixing rules, mostly one-fluid type, might severely degrade the performance of SAFT. A more promising SAFT EOS was presented by Tang and Lu,[24] using the first-order mean spherical approximation (FMSA). FMSA has its foundation in an analytical solution of the Ornstein–Zernike (OZ) equation,[25,26] leading to the availability of both the EOS and structure information such as radial distribution function (RDF) for the pure LJ fluid[27-29] and their mixtures.[30-32] The new EOS is explicit, analytical, and fully predictive outside the critical region. Uniquely, artificially imposed mixing rules are no longer required in the FMSA–SAFT.

In the critical region, however, the FMSA–SAFT fails to predict pressure–volume–temperature (P–V–T) properties of fluids just like almost all other mean-field theories. When approaching the critical region, density distribution is increasingly inhomogeneous[33,34] or density fluctuation wavelength is increasingly long ranged to the critical point.[35-37] RDF in the EOS is a key function to account for density fluctuation. Nevertheless, because of the approximations in those theories, the fluctuation distance in the RDF is only several times the molecular diameter, which does not exhibit any macroscopical characteristic. The failure of the mean-field theories occurs because the density fluctuation is not treated macroscopically. A homogeneous theory is valid only after the inhomogeneity is taken fully into account.

In recent years, many efforts have been made to describe the global VLE of fluid mixture. The crossover theory developed by Sengers and coworkers[38-40] and by Kiselev and coworkers[41-46] incorporates the scaling laws close to the critical point into universal thermodynamic model and yields a correct critical exponent. However, several parameters are required to fit experimental data for each system. Very recently, Gospodinov and Escobedo[47] used the histogram reweighting method to cross over from the classical to the scaled equation. It was shown that the histograms provided a good approximation to simulations results. Another method is the hierarchical reference theory[48] in which the density fluctuations are considered in the solution of optimized random-phase approximation of the OZ equation. Although it has been extended to fluid mixtures[49-51] and seems to be a promising theory, the mathematical complexity limits its practical applications.

The RG theory, originally proposed by Wilson[52,53] for Ising spins and lattice gas, was developed by White and coworkers[54-59] and later improved by Lue and Prausnitz[60,61] and Tang and coworkers.[62,63] The theory accounts properly for the influence of the critical fluctuations in density and provides a valid prescription to describe fluid behavior both inside and outside the critical region. Further application of Lue and Prausnitz's method was the combination of the RG theory with equation of state for chain fluids (EOSCF) by Jiang and Prausnitz.[64-66] They developed a crossover EOS for pure chain fluids and mixtures. Cai and Prausnitz,[67] on the other hand, extended the RG transform to those systems with a continuous distribution of molecular weight through a cubic EOS. Very recently, Llovell et al.[68] applied the RG transform to correcting the LJ–SAFT model around the critical region for a single component. Although these RG developments have shown good agreement with experiment data, their underlying deficiencies are nonnegligible. For instance, far from the critical region, the two later EOSs were constructed through some empirical fittings and there is no structure information. When extended to mixtures, the mixing rule is needed and the cross-parameter k_{ij} has to be fitted from experimental data. Near the critical region, almost all these methods used the original van der Waals (VDW) assumption to subtract the contribution from long-wavelength density fluctuation, neglecting any structure information. The treatment does not match with the accompanying EOS, whose performance is far better than the VDW equation outside the critical region.

Based on the earlier idea of extensive and nonextensive free energy,[62] we recently decomposed the density fluctuation into the mean-field term, the amplitude term, and the frequency term for extending White's RG theory to chain molecules.[69] Even though the frequency or nonextensive term remains to be the VDW type, the underlying mathematical process paves the way to develop the RG transform beyond the primitive assumption. As mentioned before,[62] inhomogeneity is the fundamental behind unusual critical behavior and it will make much more sense if its treatment can be carried out within the framework of today's rapidly developing density functional theory (DFT). Very recently, FMSA[70,71] has been used very successfully to study a number of inhomogeneous behaviors such as fluids around walls and around colloidal particles. These studies show that direct correlation function (DCF) plays the dominating role and a crude approximation to the function such as that in the VDW theory could be very disappointing. Uniquely, FMSA can provide an analytical and reliable DCF for almost all intermolecular potentials,[72] which is the key advantage over all other methods. Therefore, it is very appealing to apply the developed DCF to the RG theory, with all the elements systematically derived from FMSA.

In this work, we reformulate our RG transform for pure fluids and mixtures within DFT. Inside the critical region, we use DCF, instead of VDW's original intermolecular potential, to account for the nonextensive contribution. We apply the FMSA outside the critical region, whose mixture version is fully free from any mixing rules and other empirical assumptions. Our new model needs no other adjustable parameters

except the original three microscopic parameters for pure fluids (segment number m, segment diameter σ, and segment dispersion energy ε), which were regressed before outside the critical region.[29] In addition to real mixtures, we compare the RG results with available molecular simulation data for binary mixtures to illustrate its predictive ability.

A New RG Transform within DFT

The central theme in the critical region is the nonextensive concept[62] for physical properties, which is directly contrasted to our classical extensive way to handle phase split; *extensive* is here referring to a physical property in a small scope expandable to the whole space in a proportional manner, whereas *nonextensive* means such an expansion invalid. Within the context of DFT, *nonextensive* is identical to *nonlocal*, except that the latter is introduced by an external force, whereas the former is brought in with phase split or density fluctuation. To address these concepts mathematically, the nonextensive or nonlocal free energy with a density distribution of $\rho(\mathbf{r})$ can be expanded efficiently to second order as[70]

$$\beta F[\rho(\mathbf{r})] = \beta \int f[\rho(\mathbf{r}_1)]d\mathbf{r}_1 = \beta F_0(\rho_b) + \beta\mu_0 \int \Delta\rho(\mathbf{r}_1)d\mathbf{r}_1 - \frac{1}{2}\int c_0(\mathbf{r}_1-\mathbf{r}_2)\Delta\rho(\mathbf{r}_1)\Delta\rho(\mathbf{r}_2)d\mathbf{r}_1 d\mathbf{r}_2 \quad (1)$$

where subscript 0 stands for the reference or the homogeneous bulk fluid in this case, $\Delta\rho(\mathbf{r}) = \rho(\mathbf{r}) - \rho_0$, $f[\rho(\mathbf{r})]$ is the free energy density, μ_0 is the chemical potential, and $c_0(\mathbf{r})$ is the DCF. The corresponding expansion for the extensive or local free energy is

$$\beta F_0[\rho(\mathbf{r})] = \beta \int f_0[\rho(\mathbf{r}_1)]d\mathbf{r}_1 = \beta F_0(\rho_b) + \beta\mu_0 \int \Delta\rho(\mathbf{r}_1)d\mathbf{r}_1 - \frac{1}{2}\int c_0(\mathbf{r}_1-\mathbf{r}_2)\delta(\mathbf{r}_1-\mathbf{r}_2)\Delta\rho(\mathbf{r}_1)\Delta\rho(\mathbf{r}_2)d\mathbf{r}_1 d\mathbf{r}_2 \quad (2)$$

where $\delta(\mathbf{r})$ is the Dirac function, which is responsible for removing any fluctuation correlations. Focusing on the difference between the nonlocal and local free energy, as indicated by subscript D, we obtain

$$\beta F_D[\rho(\mathbf{r})] = -\frac{1}{2}\int [c_0(\mathbf{r}_1-\mathbf{r}_2) - \tilde{c}_0(0)\delta(\mathbf{r}_1-\mathbf{r}_2)]\Delta\rho(\mathbf{r}_1)\Delta\rho(\mathbf{r}_2)d\mathbf{r}_1 d\mathbf{r}_2 = -\frac{1}{2}\frac{1}{(2\pi)^3}\int [\tilde{c}_0(\mathbf{k}) - \tilde{c}_0(0)]\Delta\tilde{\rho}^2(\mathbf{k})d\mathbf{k} \quad (3)$$

where the tilde represents the three-dimensional Fourier transform, in which

$$\tilde{c}_0(\mathbf{k}) = \iiint c_0(r)e^{-i\mathbf{kr}}d\mathbf{r} = \frac{4\pi}{k}\int_0^\infty \sin(kr)rc_0(r)dr$$

an even function of k. Further applying the following expansion

$$\tilde{c}_0(\mathbf{k}) - \tilde{c}_0(0) = -4\pi C_4 k^2 + \cdots \quad (4)$$

and assuming that the density fluctuation can be represented by wave packets as

$$\Delta\rho(\mathbf{r}) = \sqrt{2}\,x\cos(\mathbf{k}_c\cdot\mathbf{r}) \quad (5)$$

or

$$\Delta\tilde{\rho}(\mathbf{k}) = (2\pi)^3\sqrt{2}\,x\frac{\delta(\mathbf{k}-\mathbf{k}_c)+\delta(\mathbf{k}+\mathbf{k}_c)}{2} \quad (6)$$

we can explicitly obtain

$$\beta F_D[\rho(\mathbf{r})] = (2\pi)^4 C_4 x^2 k_c^2 \delta(\vec{0}) \quad (7)$$

in which the nth moment of DCF is defined

$$C_n = \frac{1}{(n-1)!}\int_0^\infty c(r)r^n dr \quad (8)$$

where x is the fluctuation amplitude and k_c is the wave vector. The corresponding difference between the two free energy densities is thus given by

$$\beta f_D[\rho(\mathbf{r})] = (2\pi)C_4 x^2 k^2 \quad (9)$$

after realizing that within a macroscopic volume of V

$$\delta(\vec{0}) = \frac{V}{(2\pi)^3} \quad (10)$$

Although the above derivation undergoes some complex mathematics, the result is quite simple and concise: it is proportional to the square of both wave amplitude and frequency. In the VDW theory, DCF is simply asserted as

$$c(r) = \begin{cases} -\beta u(r) & r \geq 1 \\ 0 & r < 1 \end{cases} \quad (11)$$

and Eq. 9 reduces fully to those used in previous RG transforms. Therefore Eq. 9 can be viewed as a fundamental extension to the VDW theory.

With the availability of $f_D[\rho(\mathbf{r})]$, the remaining operations can proceed in a fashion similar to that of White's work,[55,56] yielding

$$f_n(\rho) = f_{n-1}(\rho) + \delta f_n(\rho) \quad (12)$$

with

$$f_0(\rho) = f_{\text{ref}}(\rho) \tag{13}$$

$$\delta f_n(\rho) = -\frac{1}{\beta V_n} \times \ln\left[\frac{\int_0^{\rho} dx \exp\{-V_n[\beta f_{n-1,D}(\rho, x) + 2\pi C_{4,att} x^2 k_n^2]\}}{\int_0^{\rho} dx \exp\{-V_n[\beta f_{n-1,D}(\rho, x) + 2\pi C_{2,att} x^2]\}}\right] \tag{14}$$

and

$$f_{n-1,D}(\rho, x) = \frac{f_{n-1}(\rho + x) + f_{n-1}(\rho - x)}{2} - f_{n-1}(\rho) \tag{15}$$

In Eq. 14 we have assumed that the wave-frequency contribution comes only from intermolecular attraction because attraction is the primary factor behind phase split. Strictly said, as shown in Eq. 9, C_4 should be used in the RG transform but the repulsive part is rather small. Furthermore, $C_{4,att}$ of the FMSA is close to that of the VDW theory at low densities but substantially deviates from the latter at high densities. Importantly, the new formulation exclusively unifies classical EOS, RG theory, and DFT in one framework.

For N-component chain mixtures, the fluctuation variables will be molecular densities of all the components or $\vec{\rho} = \{\rho_1, \ldots, \rho_N\}$. The RG transform derived above is equally applicable after substituting ρ with $\vec{\rho}$ and

$$\delta f_n(\vec{\rho}) = -\frac{1}{\beta V_n} \times \text{Ln}\left[\frac{\int_0^{\rho_0} \cdots \int_0^{\rho_N} dt_1 \cdots dt_N \exp\{-V_n[\beta f_{n-1,D}(\vec{\rho}, \vec{t}) + 2\pi \sum_i \sum_j C_{4,att,ij} m_i m_j t_i t_j k_{ij,n}^2]\}}{\int_0^{\rho_0} \cdots \int_0^{\rho_N} dt_1 \cdots dt_N \exp\{-V_n[\beta f_{n-1,D}(\vec{\rho}, \vec{t}) + 2\pi \sum_i \sum_j C_{2,att,ij} m_i m_j t_i t_j]\}}\right] \tag{16}$$

where

$$f_{n-1,D}(\vec{\rho}, \vec{t}) = \frac{f_{n-1}(\vec{\rho} + \vec{t}) + f_{n-1}(\vec{\rho} - \vec{t})}{2} - f_{n-1}(\vec{\rho}) \tag{17}$$

and m_i is the chain length of component i.

In our calculation, $f_{\text{ref}}(\rho)$ is the reference free energy density of FMSA–SAFT,[31] as detailed later on. The average volumes of the phase-space cell V_n used in Eq. 16 are chosen to be a function of wavelength $V_n = (\lambda_n)^3$ with $\lambda_n = 3^{n-1}\lambda_1$. The initial wavelength λ_1 is assumed to be a constant of $2\sigma_{ij}$ for all the chainlike fluids. In later transforms, the fluctuation magnitude in the density wave packets is increased by $k_n = k_1/3^{n-1}$ with $k_1 = 2\pi/\lambda_1$.

LJ chains as reference

For a chain mixture with compositions x_i, number density ρ_i, segment number m_i, and segment diameter σ_i for chain i ($i = 1, \ldots, n$), we assume that two intermolecular segments interact through the LJ potential

$$u_{ij}(r) = 4\varepsilon_{ij}\left(\frac{\sigma_{ij}^{12}}{r^{12}} - \frac{\sigma_{ij}^{6}}{r^{6}}\right) \tag{18}$$

In LJ mixtures, the unlike potential parameters are usually represented by the like potential parameters as follows

$$\sigma_{ij} = \frac{\sigma_{ii} + \sigma_{jj}}{2} \qquad \varepsilon_{ij} = \sqrt{\varepsilon_{ii}\varepsilon_{jj}} \tag{19}$$

The reduced Helmholtz free energy density can be expressed as a summation of contributions from the ideal gas, spherical segments, and chain bonding:

$$f_{\text{ref}} = f^{\text{ideal}} + f^{\text{seg}} + f^{\text{chain}} \tag{20}$$

The ideal gas contribution is given by

$$f^{\text{ideal}} = \rho \sum_{i=1}^{n} x_i \ln(\rho x_i \Lambda_i^3) - 1 \tag{21}$$

where Λ_i is the de Broglie wavelength and ρ stands for the total density.

The segment contribution is

$$f^{\text{seg}} = m f^{\text{ref}_0} \tag{22}$$

where the superscript ref_0 represents the LJ reference mixtures and m is the average chain length with $m = \sum_{i=1}^{n} x_i m_i$. The Helmholtz free energy density for the reference term has been well developed[30]

$$f^{\text{ref}_0} = f_{\text{rep}}^{\text{ref}} + f_1^{\text{ref}} + f_2^{\text{ref}} \tag{23}$$

with

$$f_{\text{rep}}^{\text{ref}} = f_0^{\text{ref}} - 2\pi\rho^2 \sum_i \sum_j x_i x_j g_{0,ij}(R_{ij}) R_{ij}^2 (R_{ij} - d_{ij}) \tag{24}$$

$$f_0^{\text{ref}} = \left[\frac{\left(\frac{\pi}{2} \xi_1 \xi_2 - \xi_2^3/\xi_3^2 \right)}{\Delta} + \frac{\xi_2^3}{\xi_3^2 \Delta^2} + \frac{\xi_2^3}{\xi_3^2} \ln \Delta \right] - \rho \ln \Delta \quad (25)$$

$$f_1^{\text{ref}} = -2\pi\rho^2\beta \sum_i \sum_j x_i x_j \varepsilon_{ij} k_{1,ij} \left[G_{0,ij}(z_{1,ij}) e^{z_{1,ij}R_{ij}} - \frac{1 + z_{1,ij}R_{ij}}{z_{1,ij}^2} \right] - k_{2,ij} \left[G_{0,ij}(z_{2,ij}) e^{z_{2,ij}R_{ij}} - \frac{1 + z_{2,ij}R_{ij}}{z_{2,ij}^2} \right] + 8\pi\rho^2\beta \sum_i \sum_j x_i x_j \varepsilon_{ij} R_{ij}^3 I_{ij,\infty} - 8\pi\rho^2\beta \sum_i \sum_j x_i x_j \varepsilon_{ij} g_{0,ij}(R_{ij}) R_{ij}^3 I_{ij,1} \quad (26)$$

$$f_2^{\text{ref}} = -\pi\rho^2\beta \sum_i \sum_j x_i x_j \varepsilon_{ij} \{ k_{1,ij} [G_{1,ij}(z_{1,ij}) e^{z_{1,ij}R_{ij}}] - k_{2,ij} [G_{2,ij}(z_{2,ij}) e^{z_{2,ij}R_{ij}}] \} - 4\pi\rho^2\beta \sum_i \sum_j x_i x_j \varepsilon_{ij} g_{1,ij}(R_{ij}) R_{ij}^3 I_{ij,1} \quad (27)$$

and

$$I_{ij,\infty} = \frac{1}{9} \left(\frac{\sigma_{ij}}{R_{ij}} \right)^{12} - \frac{1}{3} \left(\frac{\sigma_{ij}}{R_{ij}} \right)^{6} \quad (28)$$

$$I_{ij,1} = \frac{1}{9} \left(\frac{\sigma_{ij}}{R_{ij}} \right)^{12} - \frac{1}{3} \left(\frac{\sigma_{ij}}{R_{ij}} \right)^{6} + \frac{2}{9} \left(\frac{\sigma_{ij}}{R_{ij}} \right)^{3} \quad (29)$$

$$\xi_n = \sum_m \rho_m R_m^n \qquad \Delta = 1 - \frac{\pi}{6} \xi_3 \quad (30)$$

In Eqs. 24 and 26–30, $k_{1,ij}$, $k_{2,ij}$, $z_{1,ij}$, and $z_{2,ij}$ are constants related to the LJ potenial parameters; R_{ij} is the Barker–Henderson diameter[73,74]; $g_{0,ij}(R_{ij})$ and $g_{1,ij}(R_{ij})$ are the RDFs at contact; and $G_{0,ij}(z_{ij})$ and $G_{1,ij}(z_{ij})$ are the Laplace transforms of hard-sphere and first-order RDFs, respectively. Details about these quantities are left in the appendix. Equation 25 is the Helmholtz free energy density of hard-sphere mixtures given by Mansoori et al.[75]

The chain-bonding term is given by

$$f^{\text{chain}} = -\rho \sum_{i=1}^{n} x_i \sum_{j=1}^{m_i - 1} \ln g_{(i,j)(i,j+1)}^{\text{ref}}(\sigma_{(i,j),(i,j+1)}) \quad (31)$$

Here the bonding site is assumed to be tangent at $\sigma_{(i,j),(i,j+1)}$, which may be relaxed, however, because of the availability of the FMSA RDF. Because the RDF accuracy dramatically affects the performance of chain-bonding free energy,[76] it should be calculated through the more accurate simplified exponential approximation[28]

$$g_{(i,j),(i,j+1)}(\sigma_{(i,j),(i,j+1)}) = g_{0(i,j),(i,j+1)}(\sigma_{(i,j),(i,j+1)}) \times \exp[g_{1(i,j),(i,j+1)}(\sigma_{(i,j)(i,j+1)})] \quad (32)$$

Critical-point calculations

The critical point calculation for a multicomponent mixture was provided by Sadus.[77] For a multicomponent mixture, the critical point is obtained from two equations in the form of two determinants

$$W = \begin{vmatrix} \frac{\partial^2 A}{\partial V^2} & \frac{\partial^2 A}{\partial V \partial n_1} \\ \frac{\partial^2 A}{\partial V \partial n_1} & \frac{\partial^2 A}{\partial n_1^2} \end{vmatrix} \quad (33)$$

with

$$\begin{vmatrix} \frac{\partial W}{\partial V} & \frac{\partial W}{\partial n_1} \\ \frac{\partial^2 A}{\partial n_1 \partial V} & \frac{\partial^2 A}{\partial n_1^2} \end{vmatrix} = 0 \quad (34)$$

Here A is the Helmholtz free energy, V is the molar volume, $n_1 = x_1 N$, and N represents the total moles in the system. The

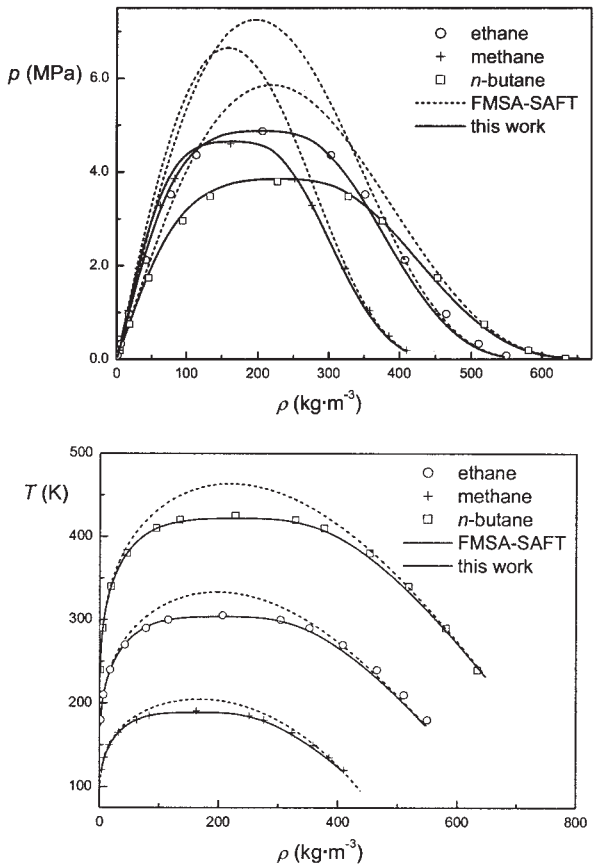

Figure 1. Vapor–liquid coexistence curves for methane, ethane and *n*-butane.

(a) p vs. ρ; (b) T vs. ρ.

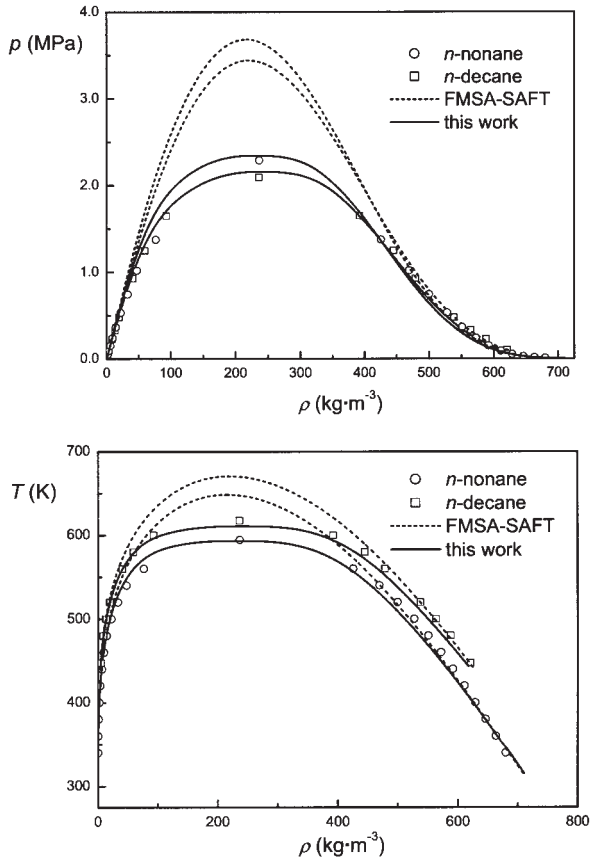

Figure 2. Vapor–liquid coexistence curves for *n*-nonane and *n*-decane.

(a) p vs. ρ; (b) T vs. ρ.

critical point can be determined by computational techniques for solving these two determinants simultaneously.

Results and Discussion

To test our new improved RG theory, we first use the new RG EOS to predict the vapor–liquid equilibria of pure fluids.

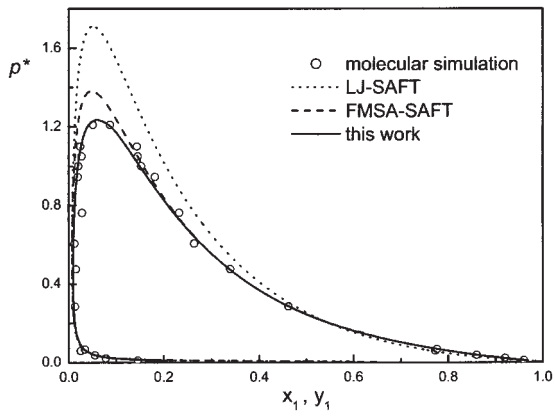

Figure 3. Reduced pressure vs. mole fraction for LJ mixture with $\sigma_{22}/\sigma_{11} = 0.5$, $\varepsilon_{22}/\varepsilon_{11} = 0.33$, $T^* = 0.75$.

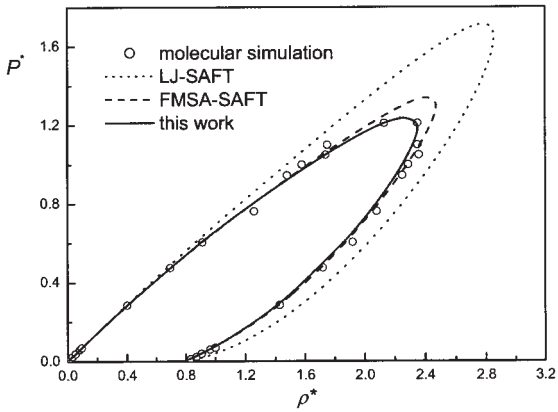

Figure 4. Reduced pressure vs. reduced density for LJ mixture with $\sigma_{22}/\sigma_{11} = 0.5$, $\varepsilon_{22}/\varepsilon_{11} = 0.33$, $T^* = 0.75$.

Then, we predict the global phase behavior for binary chain mixtures with our new EOS. We test our new EOS by molecular simulation data to validate its predictive applicability, and compare it with two other SAFT EOSs. The EOS is applied to predict critical properties and the global VLE of *n*-alkane mixtures. To describe the properties of chain fluid mixtures of *n*-alkanes, the three microscopic parameters, that is, segment number m, segment diameter σ, and segment dispersion energy ε, for pure fluids are needed. Outside the critical region, Tang et al.[29] had regressed the three parameters for *n*-alkanes and these parameters have been proven valid in our previous RG transform,[69] by which the satisfactory critical exponents and vapor–liquid coexistence curves were obtained. To maintain the consistence, we adopt the same set of microscopic parameters in the RG calculation here. Therefore, the calculation is wholly predictive because no adjustable parameters and no mixing rules are needed in this work. Note that this feature is hardly expected for other EOSs.

Application for pure fluids

The results for methane, ethane, *n*-butane, *n*-nonane, and *n*-decane are depicted in Figures 1 and 2. The experimental data are from Smith and Srivastava.[78] We can see that the EOS

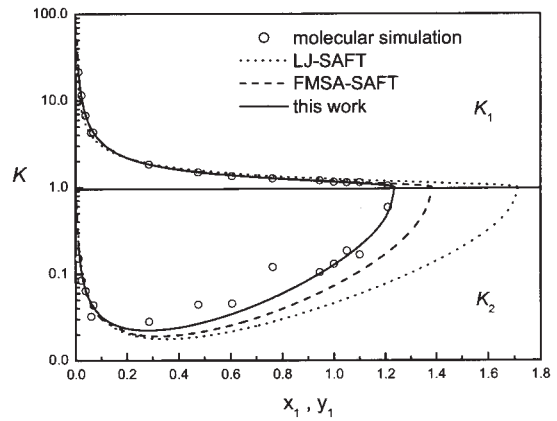

Figure 5. Equilibrium ratios for LJ mixture with $\sigma_{22}/\sigma_{11} = 0.5$, $\varepsilon_{22}/\varepsilon_{11} = 0.33$, $T^* = 0.75$.

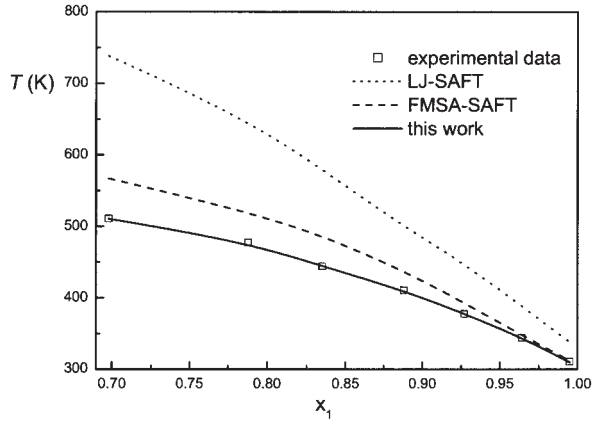

Figure 6. Comparison of critical temperature calculation results for $C_2H_6(1)$–n-$C_{10}H_{22}(2)$ mixtures.

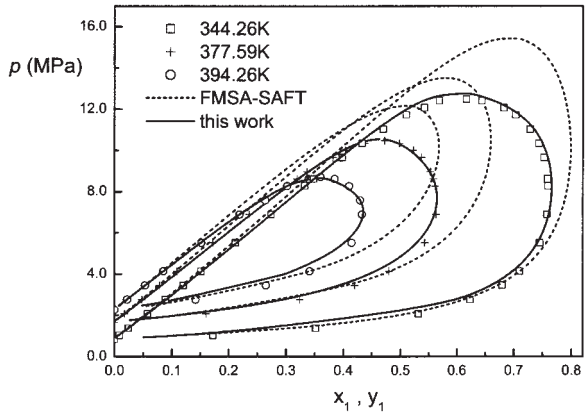

Figure 8. Vapor–liquid equilibria for $CH_4(1)$–n-$C_4H_{10}(2)$ mixtures.

yields satisfactory results for pure fluids. Most of the fluids have average relative derivation of about 1–3% for saturated pressure and saturated liquid density up to the critical point, whereas the original FMSA–SAFT predicts the critical pressure too high compared to the experimental data.

Test with molecular simulation

Theories provide a simple and flexible way for obtaining phase-coexistence envelopes of mixtures in a short time. However, its predictive applicability has to be tested to find the range of their applicability. When dealing with a specific intermolecular potential, such as the LJ fluid, the only way to test theories is to compare them with simulation data, which can in principle represent exactly the behavior of a system. We calculate VLE and compare our results with those of computer simulation. Figures 3 and 4 give the relations of reduced pressure vs. composition and vs. density, respectively, for the LJ mixture with pair potential parameters $\sigma_{22}/\sigma_{11} = 0.5$, $\varepsilon_{22}/\varepsilon_{11} = 0.33$ at a reduced temperature of $T^* (=kT/\varepsilon_{11}) = 0.75$. Figure 5 shows the corresponding equilibrium ratios defined by $K_i = y_i/x_i$. In these three figures, the results from computer simulation,[3] LJ–SAFT, FMSA–SAFT, and our new EOS are depicted simultaneously. For this mixture, unlike potential parameters are by default determined with the Lorentz–Berthelot approximation.[79] The two components have very different sizes and different potentials. It is evident that for this asymmetric mixture, the three methods yield different results. Outside the critical region, one can see that for vapor branches the LJ–SAFT performs nearly as well as the FMSA–SAFT and for liquid branches the two theories show considerable differences. The LJ–SAFT deviates systematically from computer simulation data by overestimating liquid densities as well as compositions at high pressures, whereas the FMSA–SAFT performs much better. As thoroughly discussed before,[31] these LJ–SAFT deficiencies come from its underlying mixing rule, which is not required at all in our FMSA–SAFT. With a critical point far away from simulation results and those deficiencies outside the critical region, we feel that establishing a global EOS for mixtures through LJ–SAFT + RG is very costly, if not impossible, despite its recent implementation for pure fluids.[68] The original FMSA–SAFT, in spite of giving better critical values, remains a mean-field type and overestimates the critical point as well as the surrounding region. In contrast, our new EOS—based on FMSA and RG theories, in consideration of the inhomogeneity and the long-range density fluctuations of fluid mixtures—is capable of predicting the critical point correctly and the exaggerated critical loop is successfully suppressed.

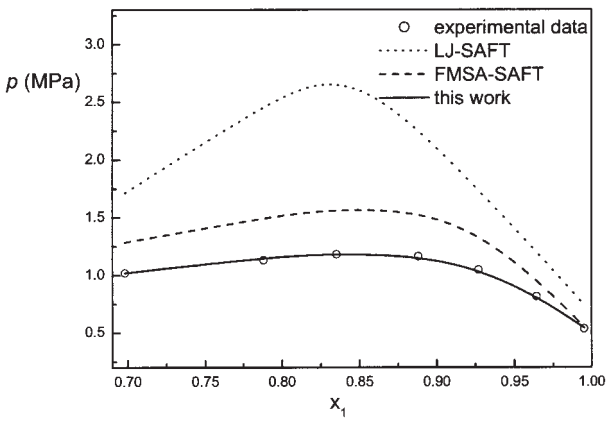

Figure 7. Comparison of critical pressure calculation results for $C_2H_6(1)$–n-$C_{10}H_{22}(2)$ mixtures.

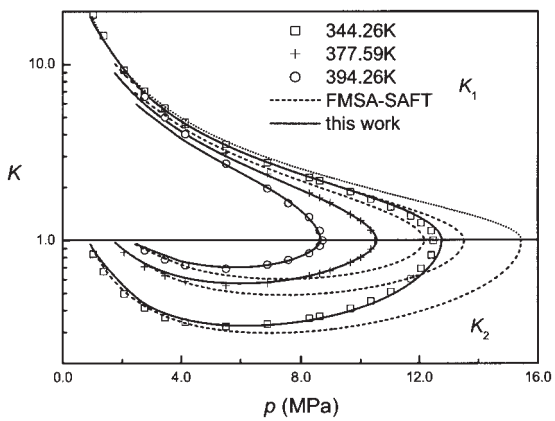

Figure 9. Equilibrium ratios for $CH_4(1)$–n-$C_4H_{10}(2)$ mixtures.

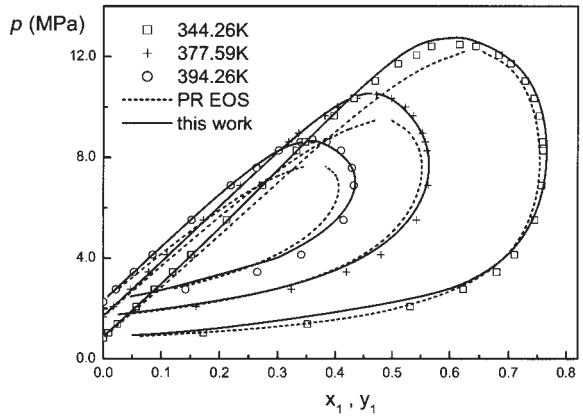

Figure 10. A comparison between phase envelopes calculated from the PR EOS and from this work for C_2H_6(1)–*n*-$C_{10}H_{22}$(2) mixtures.

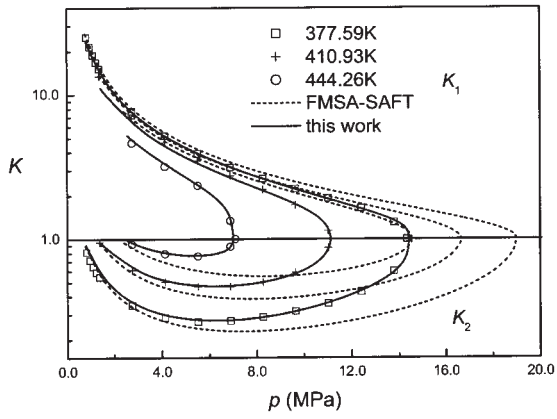

Figure 12. Equilibrium ratios for CH_4(1)–*n*-C_5H_{12}(2) mixtures.

This example strongly suggests that the FMSA + RG can faithfully handle mixture global behavior and its applications to real mixtures will be more comfortable.

Prediction of the critical properties

The ethane/*n*-decane binary system is given as an example because it is an asymmetric system and the prediction of its critical properties is more difficult than that of symmetric systems. The predicted critical temperature and pressure lines with both the SAFT EOS and the new EOS are shown in Figures 6 and 7, respectively. The open points represent the experimental data.[80] From Figures 6 and 7, it is evident that the LJ–SAFT overestimates both the critical temperatures and pressures, whereas the FMSA–SAFT yields much smaller deviations compared with the experimental data than LJ–SAFT. In both cases, the FMSA–SAFT + RG correction yields excellent critical lines.

Phase equilibria for binary mixtures with the new EOS

Figure 8 shows the prediction results of vapor–liquid equilibria for a binary methane/*n*-butane mixture; Figure 9 shows the corresponding equilibrium ratio of the mixture. Three isotherms of the binary system were plotted. The FMSA–SAFT yields accurate results below the critical pressures. However, the deviation between the calculated and the experimental data increases closing to the critical point. This deviation is caused by the overestimation of the critical temperature and pressure of the pure *n*-alkanes by the method. On the contrary, the new EOS can predict the correct critical properties for each pure component of the binary system as well as the whole VLE. As a comparison, we also show the results from the PR EOS in Figure 10, which is widely accepted in the simulation industry. It is evident that the cubic EOS yields rather truncated envelopes in all three temperatures and this behavior may hold for other cubic EOSs if without extra parameters. Figure 11, similar to Figure 8, yields prediction results for methane/*n*-pentane binary mixtures, in which the experimental data for VLE are from Knapp et al.[80] Figure 12 yields the corresponding equilibrium ratio of the system, whose agreement is as good as that in Figure 9. Three isotherms of the binary system were plotted. Compared with Jiang and Prausnitz,[66] the average absolute deviations of the calculation results are similar, whereas our EOS needs no other adjustable and mixing parameters.

To further illustrate the new EOS, the highly asymmetric binary mixtures are investigated. The VLE and the corresponding equilibrium ratio for ethane/*n*-decane mixtures is predicted and plotted in Figures 13 and 14, respectively. The VLEs for

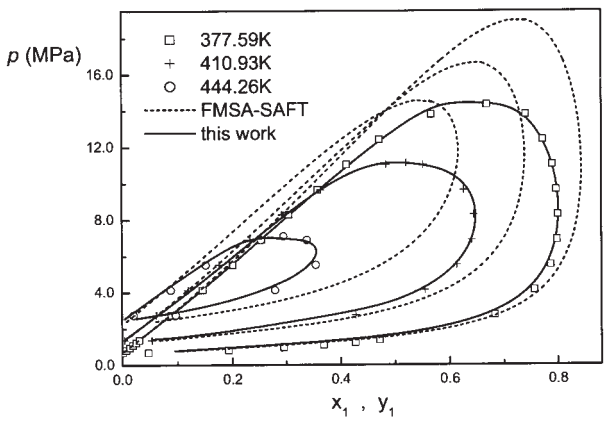

Figure 11. Vapor–liquid equilibria for CH_4(1)–*n*-C_5H_{12}(2) mixtures.

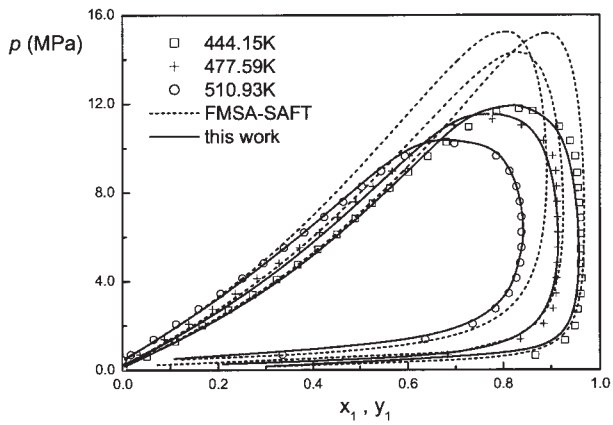

Figure 13. Vapor–liquid equilibria for C_2H_6(1)–*n*-$C_{10}H_{22}$(2) mixtures.

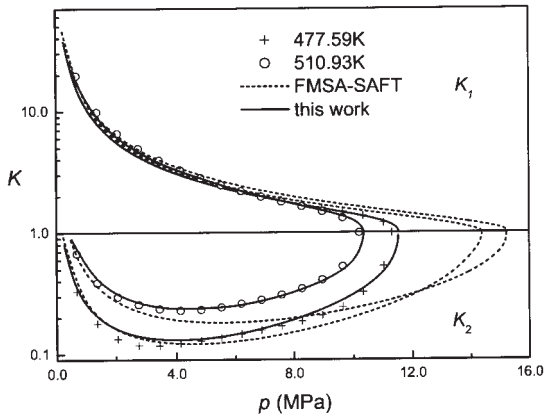

Figure 14. Equilibrium ratios for C_2H_6(1)–*n*-$C_{10}H_{22}$(2) mixtures.

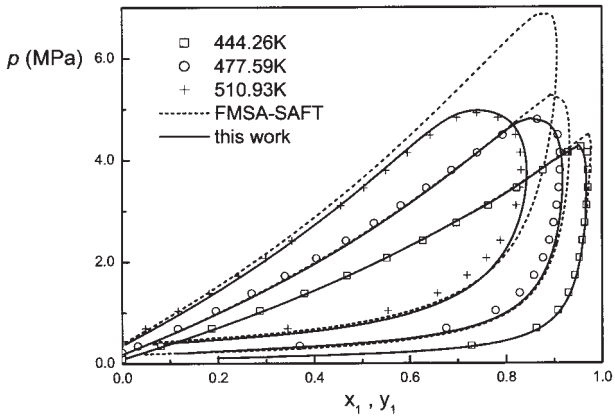

Figure 16. Vapor–liquid equilibria for C_4H_{10}(1)–*n*-$C_{10}H_{22}$(2) mixtures.

methane/*n*-nonane and *n*-butane/*n*-decane are depicted in Figures 15 and 16, respectively. The results are in good agreement with experimental data,[80] whereas the original FMSA–SAFT is unable to predict the correct thermodynamic properties inside the critical region.

Conclusions

In this work, the RG theory is integrated with DFT to describe the nonextensive free energy in the critical region of both pure chains and chain mixtures. The new RG theory is consistent both inside and outside the critical region. Outside the critical region, where density fluctuations are small, the much improved and explicit analytical RDF of FMSA provides an accurate description of fluid structure for establishing the SAFT EOS. Inside the critical region, density fluctuations are long ranged and the FMSA DCF is essential to account for their macroscopic contribution. Comparisons with molecular simulation data have confirmed the high fidelity of the developed EOS. Uniquely, traditional mixing rules are no longer required. These features are certainly beneficial in prediction of real fluid mixtures.

The predictive capability of the newly proposed EOS for global vapor–liquid phase equilibria of chain fluid mixtures is addressed. The present work shows that the combination of RG theory with the FMSA–SAFT is a good approach for developing a new EOS capable of predicting fluid mixture properties both inside and outside the critical region. The calculated results demonstrate that the EOS thus obtained can give satisfactory results even for highly asymmetric mixtures, thus clearly illustrating the power of the improved RG theory inside the critical region as well as the power of the FMSA–SAFT outside the critical region.

As a result, the combination of the two theories provides a powerful tool for predicting thermodynamic properties of practically systems of interest in the whole region. Although this work has shown the prediction capability of the VLE for binary mixtures of *n*-alkanes, we can with confidence predict global VLE for systems containing more than two components, which is often met in the chemical industry. The present difficulty is the multidimensional integration in the RG theory. Further investigation about this integral is needed in the future.

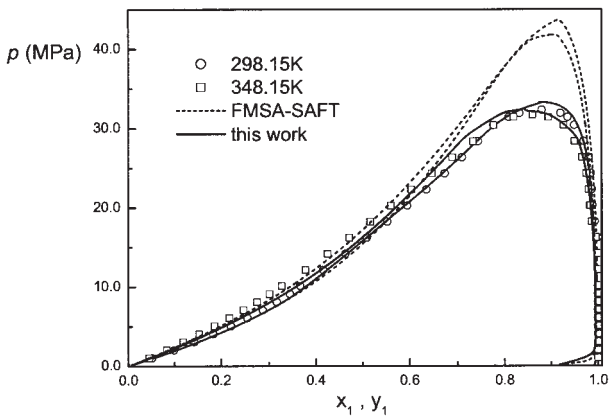

Figure 15. Vapor–liquid equilibria for CH_4(1)–*n*-C_9H_{20}(2) mixtures.

Acknowledgments

The authors gratefully acknowledge the financial support of the Natural Science Foundation of BUCT (Contract QN0402), the Natural Science Foundation of China (Contract 20476003), and the Specialized Research Fund for the Doctoral Program of Higher Education of China (Contract 20040010002).

Literature Cited

1. Harismiadis VI, Kourtras NK, Tassios DP, Panagiotopoulos AZ. How good is conformal solutions theory for binary phase equilibrium predictions? *Fluid Phase Equilib.* 1991;65:1-18.
2. Vrabec J, Fischer J. Vapour liquid equilibria of Lennard–Jones mixtures from the *NpT* plus test particle method. *Fluid Phase Equilib.* 1995;112:173-197.
3. Georgoulaki AM, Ntouros IV, Tassios DP, Panagiotopoulos AZ. Phase equilibrium of binary Lennard–Jones mixtures: Simulation and van der Waals 1-fluid theory. *Fluid Phase Equilib.* 1994;100:153-170.
4. Canongia Lopes JN, Tildesley DJ. Multiphase equilibria in binary Lennard–Jones mixures: Phase diagram simulation. *Mol Phys.* 1999; 96:1649-1658.
5. Sadus RJ. Molecular simulation of the phase behavior of ternary fluid mixtures: The effect of a third component on vapor–liquid and liquid–liquid coexistence. *Fluid Phase Equilib.* 1999;157:169-180.
6. Redlich O, Kwong JNS. On the thermodynamics of solutions. V: An equation of state: Fugacities of gaseous solutions. *Chem Rev.* 1949; 44:233-244.
7. Soave G. Equilibrium constants from a modified Redlich–Kwong equation of state. *Chem Eng Sci.* 1972;27:1197-1203.

8. Peng D, Robinson DB. A new two-constant equation of state. *Ind Eng Chem Fundam.* 1976;15:59-64.
9. Wei YS, Sadus RJ. Equation of state for the calculation of fluid-phase equilibria. *AIChE J.* 2000;46:169-196.
10. Span R, Wanger W, Lemmon EW, Jacobsen RT. Multiparameter equations of state—Recent trends and future challenges. *Fluid Phase Equilib.* 2001;183-184:1–20.
11. Fotouh K, Shukla K. An improved perturbation theory and van der Waals one-fluid theory of binary fluid mixture: Part 1. Total and excess thermodynamic properties. *Fluid Phase Equilib.* 1997;127:45-70.
12. Fotouh K, Shukla K. An improved perturbation theory and van der Waals one-fluid theory of binary fluid mixture: Part 2. Phase equilibria. *Fluid Phase Equilib.* 1997;137:1-16.
13. Chapman WG, Gubbins KE, Jackson G, Radosz M. SAFT: equation-of-state solution model for associating fluid. *Fluid Phase Equilib.* 1989;52:31-38.
14. Jacson G, Chapman WG, Gubbins KE. Phase equilibria of associating fluids spherical molecules with multiple bonding sites. *Mol Phys.* 1988;65:1-31.
15. Chapman WG, Gubbins KE, Jackson G, Radosz M. New reference equation of state for associating liquids. *Ind Eng Chem Res.* 1990;29: 1709-1721.
16. Huang SH, Radosz M. Equation of state for small, large, polydisperse and associating molecules. *Ind Eng Chem Res.* 1990;29:2284-2294.
17. Huang SH, Radosz M. Equation of state for small, large, polydisperse and associating molecules: Extension to fluid mixtures. *Ind Eng Chem Res.* 1991;30:1994-2005.
18. Kraska T, Gubbins KE. Phase equilibria calculations with a modified SAFT equation of state. 1. Pure alkanes, alkanols, and water. *Ind Eng Chem Res.* 1996;35:4727-4737.
19. Kraska T, Gubbins KE. Phase equilibria calculation with a modified SAFT equation of state. 2. Binary mixtures of *n*-alkanes, 1-alkanols, and water. *Ind Eng Chem Res.* 1996;35:4738-4746.
20. Blas FJ, Vega LF. Prediction of binary and ternary diagrams using the statistical associating fluid theory (SAFT) equation of state. *Ind Eng Chem Res.* 1998;37:660-674.
21. Gross J, Sadowski G. Application of perturbation theory to hard-chain reference fluids: An equation of state for square-well chains. *Ind Eng Chem Res.* 2001;40:1244-1260.
22. Gil-Villegas A, Galindo A, Whitehead PJ, Mills SJ, Jackson G, Burges AN. Statistical associating fluid theory for chain molecules with attractive potentials of variable range. *J Chem Phys.* 1997;106:4168-4186.
23. Tumakaka F, Sadowski G. Application of the perturbed-chain SAFT equation of state to polar systems. *Fluid Phase Equilib.* 2004;217:233-239.
24. Tang YP, Lu BCY. A study of associating Lennard–Jones chains by a new reference radial distribution function. *Fluid Phase Equilib.* 2000; 171:27-44.
25. Tang YP, Lu BCY. Analytical solution of the Ornstein–Zernike equation for mixtures. *Mol Phys.* 1995;84:89-103.
26. Tang YP, Lu BCY. A New solution of the Ornstein–Zernike equation from the perturbation theory. *J Chem Phys.* 1993;99:9828-9835.
27. Tang YP, Lu BCY. An Analytical analysis of the square well fluid behavior. *J Chem Phys.* 1994;100:6665-6671.
28. Tang YP, Lu BCY. Analytical description of the Lennard–Jones fluid and its application. *AIChE J.* 1997;43:2215-2226.
29. Tang YP, Wang Z, Lu BCY. Thermodynamic calculation of linear chain molecules using a SAFT model. *Mol Phys.* 2001;99:65-76.
30. Tang YP, Lu BCY. Analytical equation of state for Lennard–Jones mixtures. *Fluid Phase Equilib.* 1998;146:73-92.
31. Tang YP, Lu BCY. Phase equilibria study of Lennard–Jones mixtures by an analytical equation of state. *Fluid Phase Equilib.* 1999;165:183-196.
32. Tang YP. SAFT model for associating LJ chain mixture. *Mol Phys.* 2002;100:1033-1047.
33. Kajimoto O. Solvation in supercritical fluids: Its effects on energy transfer and chemical reactions. *Chem Rev.* 1999;99:355-390.
34. Tucker SC. Solvent density inhomogeneities in supercritical fluids. *Chem Rev.* 1999;99:391.
35. Senger JV, Levelt Sengers JMH. Thermodynamic behavior of fluids near the critical point. *Annu Rev Phys Chem.* 1986;37:189-222.
36. Fisher ME. Renormalization of critical theory: Its basis and formulation in statistical physics. *Rev Mod Phys.* 1998;70:653-681.
37. Levelt Sengers JMH. Mean-field theories, their weaknesses and strength. *Fluid Phase Equilib.* 1999;158/160:3-17.
38. Edison TA, Anisimov MA, Sengers JV. Critical scaling laws and an excess Gibbs energy model. *Fluid Phase Equilib.* 1998;150/151:429-438.
39. Anisimov MA, Povodyrev AA, Sengers JV. Crossover critical phenomena in complex fluids. *Fluid Phase Equilib.* 1995;158/160:537–547.
40. Povodyrev AA, Anisimov MA, Sengers JV. Crossover Flory model for phase separation in polymer solutions. *Physica A.* 1999;264:345-369.
41. Kiselev SB. Cubic crossover equation of state. *Fluid Phase Equilib.* 1998;147:7-23.
42. Kiselev SB, Ely JF. Crossover SAFT equation of state: Application for normal alkanes. *Ind Eng Chem Res.* 1999;38:4993-5004.
43. Kiselev SB, Rainwater JC. Enthalpies, excess volumes, and specific heats of critical and supercritical binary mixture. *J Chem Phys.* 1998; 109:643-657.
44. Kiselev SB, Ely JF. Simplified crossover SAFT equation of state for pure fluids and fluids mixtures. *Fluid Phase Equilib.* 2000;174:93-113.
45. Kiselev SB, Ely JF, Lue L, Elliott JR. Computer simulations and crossover equation of state of square-well fluids. *Fluid Phase Equilib.* 2002;200:121-149.
46. Kiselev SB, Rainwater JC, Huber ML. Binary mixtures in and beyond the critical region: Thermodynamic properties. *Fluid Phase Equilib.* 1998;150/151:469-478.
47. Gospodinov ID, Escobedo FA. Bridging continuum and statistical thermodynamics via equations of state and the density of states. *J Chem Phys.* 2004;120:10699-10710.
48. Parola A, Reatto L. Hierarchical reference theory of fluids and the critical point. *Phys Rev A.* 1991;44:6600-6615.
49. Reatto L, Parola A. Liquid-state theory and the renormalization group reconciled: A theory for phase transitions in fluids. *J Phys Condens Matter.* 1996;8:9221-9232.
50. Pini D, Stell G, Hoye JS. Self-consistent approximation for fluids and lattice gases. *Int J Thermophys.* 1998;19:1029-1038.
51. Pini D, Stell G, Wilding NB. A liquid-state theory that remains successful in the critical region. *Mol Phys.* 1998;95:483-494.
52. Wilson KG. Renormalization group and critical phenomena: I. Renormalization group and the Kadanoff scaling picture. *Phys Rev B.* 1971; 4:3174-3183.
53. Wilson KG. Renormalization group and critical phenomena: II. Phase-space cell analysis of critical behavior. *Phys Rev B.* 1971;4:3184-3205.
54. Wilson KG. The renormalization group and critical phenomena. *Rev Mod Phys.* 1983;55:583-600.
55. White JA. Contribution of fluctuation to thermal properties of fluids with attractive force of limited range: Theory compared with $p\rho T$ and C_V data for argon. *Fluid Phase Equilib.* 1992;75:53-64.
56. Salvino LW, White JA. Calculation of density fluctuation contributions to thermodynamic properties of simple fluids. *J Chem Phys.* 1992;96:4559-4568.
57. White JA, Zhang S. Renormalization group theory for fluids. *J Chem Phys.* 1993;99:2013-2019.
58. White JA, Zhang S. Renormalization theory for nonuniversal thermal properties of fluids. *J Chem Phys.* 1995;103:1922-1928.
59. White JA. Lennard–Jones as a model for argon and test of extended RG calculations. *J Chem Phys.* 1999;111:9352-9356.
60. Lue L, Prausnitz JM. Renormalization group theory correlations to an approximation free-energy model for simple fluids near to and far from the critical region. *J Chem Phys.* 1998;108:5529-5536.
61. Lue L, Prausnitz JM. Thermodynamic of fluid mixtures near to and far from the critical region. *AIChE J.* 1998;44:1455-1466.
62. Tang YP. Outside and inside the critical region of the Lennard–Jones fluid. *J Chem Phys.* 1998;109:5935-5944.
63. Duan LP, Chen J, Lu JF, Li YG. Study of the critical behavior of polar fluids by renormalization group theory. *Ind Eng Chem Res.* 2002;41: 297-302.
64. Jiang J, Prausnitz JM. Equation of state for thermodynamic properties of chain fluids near-to and far-from the vapor–liquid critical region. *J Chem Phys.* 1999;111:5964-5974.
65. Jiang J, Prausnitz JM. Critical temperatures and pressures for hydrocarbon mixtures form an equation of state with renormalization-group-theory corrections. *Fluid Phase Equilib.* 2000;169:127-147.
66. Jiang J, Prausnitz JM. Phase equilibria for chain-fluid mixtures near to and far from the critical region. *AIChE J.* 2000;46:2525-2536.
67. Cai J, Prausnitz JM. Thermodynamics for fluid mixtures near to and far

from the vapor–liquid critical point. *Fluid Phase Equilib.* 2004;219: 205-217.
68. Llovell F, Pamies JC, Vega LF. Thermodynamic properties of Lennard–Jones chain molecules: Renormalization-group corrections to a modified statistical associating fluid theory. *J Chem Phys.* 2004;121: 10715-10724.
69. Mi JG, Zhong CL, Li YG, Tang YP. An improved renormalization group theory for real fluids. *J Chem Phys.* 2004;121:5372-5380.
70. Tang YP. First-order mean spherical approximation for inhomogeneous fluids. *J Chem Phys.* 2004;121:10605-10610.
71. Tang YP, Wu JZ. Model inhomogeneous van der Waals fluid using an analytical direct correlation function. *Phys Rev E.* 2004;70:011201: 1-8.
72. Tang YP. On the first-order mean spherical approximation. *J Chem Phys.* 2003;118:4140-4148.
73. Barker JA, Henderson D. Perturbation theory and equation of state for fluids: The square well potential. *J Chem Phys.* 1967;47:2856-2861.
74. Barker JA, Henderson D. Perturbation theory and equation of state for fluids: II. A successful theory of fluids. *J Chem Phys.* 1967;47:4714-4721.
75. Mansoori G, Carnahan NF, Starling KE, Leland TE. Equilibrium thermodynamic properties of the mixture of hard spheres. *J Chem Phys.* 1971;54:1523-1525.
76. Tang Y, Lu BCY. Improved expressions for the radial distribution function of hard sphere. *J Chem Phys.* 1995;103:7463-7470.
77. Sadus RJ. *High Pressure Phase Behavior of Multicomponent Fluid Mixtures*. Amsterdam, The Netherlands: Elsevier Science; 1992.
78. Smith BD, Srivastava R. *Physical Science Data: Thermodynamic Data for Pure Compounds, Part A: Hydrocarbons and Ketones*. Vol. 25. New York, NY: Elsevier; 1986.
79. Rowlinson JS, Swinton FL. *Liquids and Liquid Mixtures*. 3rd Edition. London, UK: Butterworths; 1982.
80. Knapp JR, Döring L, Oellrich, Plöcker U, Prausnitz JM. *Vapor–Liquid Equilibria for Mixtures of Low Boiling Substances* (Chemistry Data Series). Vol. VI. Frankurt, Germany: DECHEMA; 1982.

Appendix

The functions and quantities in Eq. 16 are correspondingly extended to mixtures as follows[72]:

$$c_{att,ij}(r) = c_{1,ij}(T_1^*, z_{1,ij}R_{ij}, r_{ij}/R_{ij}) - c_{1,ij}(T_2^*, z_{2,ij}R_{ij}, r_{ij}/R_{ij}) \quad \text{(A1)}$$

$$T_1^* = T^*R_{ij}/k_{1,ij} \qquad T_2^* = T^*R_{ij}/k_{2,ij}$$
$$z_{1,ij} = 2.9637/\sigma_{ij} \qquad z_{2,ij} = 14.01677/\sigma_{ij} \quad \text{(A2)}$$

$$k_{1,ij} = 2.1714\sigma_{ij}e^{z_{1,ij}(\sigma_{ij}-R_{ij})} \qquad k_{2,ij} = 2.1714\sigma_{ij}e^{z_{2,ij}(\sigma_{ij}-R_{ij})} \quad \text{(A3)}$$

$$r_{ij}/R_{ij}c_{1,ij}(T^*, z_{ij}, r_{ij}/R_{ij}) = \begin{cases} \dfrac{e^{-z_{ij}(r_{ij}-R_{ij})}}{T^*} & r_{ij} > R_{ij} \\ \dfrac{e^{-z_{ij}(r_{ij}-R_{ij})}}{T^*} - \dfrac{1}{(1-\eta)^4 z_{ij}^6 Q^2(z_{ij})T^*}\{S^2(z_{ij})e^{-z_{ij}(r_{ij}-R_{ij})} + 144\eta^2 L^2(z_{ij})e^{z_{ij}(r_{ij}-R_{ij})} \\ \quad - 12\eta^2[(1+2\eta)^2 z_{ij}^4 + (1-\eta)(1+2\eta)z_{ij}^5]r_{ij}^4/R_{ij}^4 + 12\eta[S(z_{ij})L(z_{ij})z_{ij}^2 \\ \quad - (1-\eta)^2(1+\eta/2)z_{ij}^6]r_{ij}^2/R_{ij}^2 - 24\eta[(1+2\eta)^2 z_{ij}^4 + (1-\eta)(1+2\eta)z_{ij}^5]r_{ij}/R_{ij} \\ \quad + 24\eta S(z_{ij})L(z_{ij})\} & r_{ij} \le R_{ij} \end{cases} \quad \text{(A4)}$$

$$Q(t) = \frac{S(t) + 12\eta L(t)e^{-t}}{(1-\eta)^2 t^3} \quad \text{(A5)}$$

$$S(t) = (1-\eta)^2 t^3 + 6\eta(1-\eta)t^2 + 18\eta^2 t - 12\eta(1+2\eta) \quad \text{(A6)}$$

$$L(t) = (1+\eta/2)t + 1 + 2\eta \qquad \eta = \frac{\pi}{6}\sum_m \rho_m R_m^3 \quad \text{(A7)}$$

The functions and quantities in Eqs. 24 and 26–30 are defined as follows:

$$R_{ij}g_{0,ij}(R_{ij}) = \frac{R_{ij}}{\Delta} + \frac{\pi\xi_2 R_i R_j}{4\Delta^2} \quad \text{(A8)}$$

$$R_{ij}g_{1,ij}(R_{ij}) = \frac{1}{2\pi\sqrt{\rho_i\rho_j}}\sum_l\sum_k [K_{1,lk}B_{il}(z_{1,lk})B_{jk}(z_{1,lk}) - K_{2,lk}B_{il}(z_{2,lk})B_{jk}(z_{2,lk})] \quad \text{(A9)}$$

$$\{G_0(s)\}_{ij} = \frac{e^{-sR_{ij}}}{\Delta\ \det(s)}\left[\frac{1}{s^2}\left(1 + \frac{\pi\xi_3}{2\Delta}\right) + \frac{1}{s}\left(R_{ij} + \frac{\pi\xi_2 R_i R_j}{4\Delta}\right) + \frac{\pi}{2\Delta s}\sum_m \rho_m\varphi_1(R_m)(R_m - R_i)(R_m - R_j)\right] \quad \text{(A10)}$$

$$\{G_1(s)\}_{ij} = \{G_{11}(s)\}_{ij} - \{G_{12}(s)\}_{ij} \quad \text{(A11)}$$

$$\{G_{1,\gamma}(s)\}_{ij} = \sum_l\sum_k\sum_m\sum_n \times \frac{K_{\gamma,lk}B_{ml}(z_{\gamma,lk})B_{nk}(z_{\gamma,lk})B_{mi}(s)B_{nj}(s)}{s + z_{\gamma,lk}}\frac{e^{-sR_{ij}}}{2\pi\sqrt{\rho_i\rho_j}} \qquad \gamma = 1, 2 \quad \text{(A12)}$$

$$B_{ij}(s) = \delta_{ij} + 2\pi\sqrt{\rho_i\rho_j}\frac{W_{ij}(s)}{\Delta\ \det(s)} \quad \text{(A13)}$$

$$W_{ij}(s) = \varphi_2(R_i)\left(1 + \frac{\pi\xi_3}{2\Delta}\right) + \varphi_1(R_i)\left(R_{ij} + \frac{\pi\xi_2 R_i R_j}{4\Delta}\right)$$

$$+\frac{\pi}{2\Delta}\varphi_1(R_i)\sum_m \rho_m\varphi_1(R_m)(R_m-R_i)(R_m-R_j)$$

$$+\frac{\pi}{2\Delta}R_i^2\sum_m \rho_m\varphi_2(R_m)(R_j-R_m) \quad \text{(A14)}$$

$$\varphi_1(R_i)=\frac{1-sR_i-e^{-sR_i}}{s^2} \quad \text{(A15)}$$

$$\varphi_2(R_i)=\frac{1-sR_i+\frac{(sR_i)^2}{2}-e^{-sR_i}}{s^3} \quad \text{(A16)}$$

$$\det(s)=1-\frac{2\pi}{\Delta}\sum_m \rho_m\varphi_2(R_m)\left(1+\frac{\pi\xi_3}{2\Delta}\right)-\frac{2\pi}{\Delta}\sum_m \rho_m\varphi_1(R_m)$$
$$\times\left(R_m+\frac{\pi\xi_2R_m^2}{4\Delta}\right)-\frac{\pi^2}{2\Delta^2}\sum_m\sum_n \rho_m\rho_n\varphi_1(R_m)\varphi_1(R_n)(R_m-R_n)^2 \quad \text{(A17)}$$

with

$$K_{1,ij}=2\pi\sqrt{\rho_i\rho_j}\,\beta\varepsilon_{ij}k_{1,ij} \qquad K_{2,ij}=2\pi\sqrt{\rho_i\rho_j}\,\beta\varepsilon_{ij}k_{2,ij} \quad \text{(A18)}$$

and the Kronecker delta

$$\delta_{ij}=\begin{cases}1 & i=j\\ 0 & i\neq j\end{cases} \quad \text{(A19)}$$

$\beta = 1/kT$, where k is Boltzmann's constant and T is the absolute temperature.

$$R_{ij}=\frac{R_{ii}+R_{jj}}{2} \qquad R_{ii}=2\sum_j x_jd_{ij}-\sum_i\sum_j x_ix_jd_{ij} \quad \text{(A20)}$$

with

$$d_{ij}=\sigma_{ij}\frac{1+0.2977T^*}{1+0.33163T^*+0.00104774T^{*2}} \qquad T^*=kT/\varepsilon_{ij} \quad \text{(A21)}$$

Manuscript received Jan. 25, 2005, and revision received May 3, 2005.